Unification of Aeolian and Fluvial Sediment Transport Rate from Granular Physics

Thomas Pähtz [1,2,*] and Orencio Durán [3]

[1]*Institute of Port, Coastal and Offshore Engineering, Ocean College, Zhejiang University, 310058 Hangzhou, China*
[2]*State Key Laboratory of Satellite Ocean Environment Dynamics, Second Institute of Oceanography, 310012 Hangzhou, China*
[3]*Department of Ocean Engineering, Texas A&M University, College Station, Texas 77843-3136, USA*

One of the physically least understood characteristics of geophysical transport of sediments along sediment surfaces is the well-known experimental observation that the sediment transport rate Q is linearly dependent on the fluid shear stress τ applied onto the surface in air, but is nonlinearly dependent on τ in water. Using transport simulations for a wide range of driving conditions, we show that the scaling depends on the manner in which the kinetic fluctuation energy of transported particles is dissipated: via predominantly fluid drag and quasistatic contacts (linear) versus fluid drag and quasistatic and collisional contacts (nonlinear). We use this finding to derive a scaling law (asymptotically $Q \sim \tau^2$) in simultaneous agreement with measurements in water and air streams.

Turbulent shearing flows of Newtonian fluid along planetary surfaces composed of loose sediment are an important driver of sediment transport and erosion on Earth and other planets [1–6]. In particular, if the transported sediment is frequently deposited on the sediment bed underneath (i.e., if it is not suspended by the fluid turbulence), then the interplay between erosion, deposition, bed topography, and flow gives rise to a rich variety of bedforms, such as desert dunes and subaqueous ripples [6–8]. Predicting the evolution of fluid-sheared planetary surfaces thus requires a profound understanding of nonsuspended sediment transport [9–12], especially of the dependency of the transport rate Q on environmental parameters, such as the fluid shear stress τ applied onto the bed. Measurements have revealed that Q scales approximately linearly with τ in aeolian (i.e., air-driven) transport [13–15], but scales nonlinearly with τ in fluvial (i.e., liquid-driven) transport [16–19]. However, the physical origin of this difference remains controversial [20–22] and a general scaling law for Q elusive.

Here, using discrete element method-based sediment transport simulations, we show that the linear-to-nonlinear transition in the scaling of Q with τ is caused by a regime shift in the manner in which kinetic fluctuation energy of transported particles is dissipated. Via parametrizing this shift, we derive a general scaling law, valid for continuous (not intermittent) turbulent transport of nearly monodisperse sediment, in simultaneous agreement with measurements in water and air streams.

We use the numerical model of Ref. [23], which couples a discrete element method for the particle motion under gravity, buoyancy, and fluid drag with a continuum Reynolds-averaged description of hydrodynamics. Spherical particles ($\sim 10^4$) with mild polydispersity are confined in a quasi-two-dimensional domain of length

$\sim 10^3 d$ (where d is the mean particle diameter), with periodic boundary conditions in the flow direction, and interact via normal repulsion (restitution coefficient $e = 0.9$) and tangential friction (contact friction coefficient $\mu_c = 0.5$). The bottom-most particle layer is glued on a bottom wall, while the top of the simulation domain is reflective but so high that it is never reached by transported particles. The Reynolds-averaged Navier-Stokes equations are combined with a semiempirical mixing length closure that ensures a smooth hydrodynamic transition from high to low particle concentration at the bed surface and quantitatively reproduces the mean turbulent flow velocity profile in the absence of transport. Simulations with this numerical model are insensitive to e, and therefore insensitive to viscous damping, and simultaneously reproduce measurements of the rate and threshold of aeolian and viscous and turbulent fluvial transport (Figs. 1 and 3 of Ref. [21]), height profiles of relevant equilibrium transport properties (Fig. 2 of Ref. [21] and Fig. 6 of Ref. [24]), and aeolian ripple formation [25]. Details of the numerical model and its validation are described in the Supplemental Material [26].

The simulated steady, homogeneous transport conditions are characterized by three dimensionless numbers: the particle-fluid-density ratio $s \equiv \rho_p/\rho_f$, Galileo number $\mathrm{Ga} \equiv \sqrt{s\tilde{g}d^3}/\nu$ (also known as Yalin parameter [27]), and Shields number $\Theta \equiv \tau/(\rho_p\tilde{g}d)$, where $\tilde{g} \equiv (1 - 1/s)g$ is the buoyancy-reduced value of the gravitational constant g and ν the kinematic fluid viscosity. The density ratio s separates aeolian ($s \gtrsim 10$) from fluvial ($s \lesssim 10$) conditions, while Ga controls the dimensionless terminal settling velocity [i.e., $v_s/\sqrt{s\tilde{g}d} = f(\mathrm{Ga})$] [21].

We consider a Cartesian coordinate system (x, y, z), with x the horizontal coordinate in the flow direction, z the

vertical coordinate in the direction normal to the bed oriented upwards, and y the lateral coordinate. For a given simulated condition, we define the bed surface elevation z_r as the effective elevation of transported particles rebounding with the bed [22] (see the Supplemental Material [26] for the computation of physical quantities from the simulation data). From the masses (m^i) and velocities ($\mathbf{v}^i$) of all particles, numbered consecutively (upper index i), we then obtain the sediment transport rate $Q \equiv (1/\Delta)\langle \sum_i m^i v_x^i \rangle_T$ (i.e., the average total horizontal particle momentum per unit bed area), transport load $M \equiv (1/\Delta)\langle \sum_{z^i \geq z_r} m^i \rangle_T$ (i.e., the average total mass of particles transported above z_r per unit bed area), and average horizontal velocity of transported particles $\overline{v_x} \equiv Q/M$, where Δ is the area of the (x, y)-simulation domain and $\langle \cdot \rangle_T$ denotes the time average. These quantities are nondimensionalized via $Q_* \equiv Q/(\rho_p d\sqrt{s\tilde{g}d})$, $M_* \equiv M/(\rho_p d)$, and $\overline{v_{x*}} \equiv \overline{v_x}/\sqrt{s\tilde{g}d}$.

Using the definitions from the previous paragraph, the main finding of this Letter is the following relationship between Q_* and M_* (Fig. 1):

$$Q_* = M_* \overline{v_{x*t}} (1 + c_M M_*), \tag{1}$$

where $c_M = 1.7$ and a quantity's subscript t refers to its value in the limit of no transport: $\Theta \to \Theta_t(\text{Ga}, s)$ (equivalent to $M_* \to 0$). The function $\Theta_t(\text{Ga}, s)$ defines the transport threshold Shields number for given transport conditions Ga and s [21]. We find that Eq. (1) is valid for both fluvial conditions with $s^{1/2}\text{Ga} \gtrsim 80$ and aeolian conditions with $s^{1/2}\text{Ga} \gtrsim 200$ (Fig. 1), encompassing the
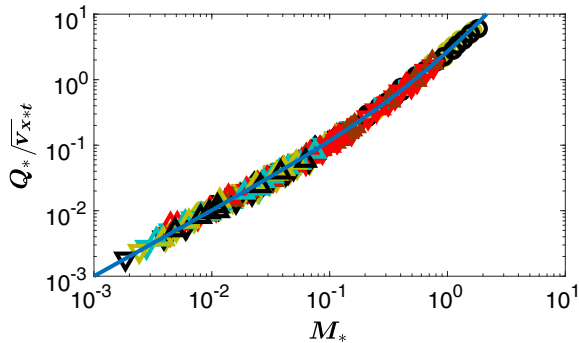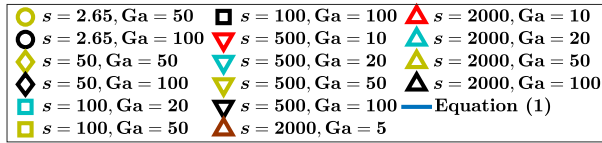
FIG. 1. $Q_*/\overline{v_{x*t}}$ versus M_*. Symbols correspond to data from numerical sediment transport simulations for various combinations of the density ratio s, Galileo number Ga, and Shields number Θ, satisfying the conditions $s^{1/2}\text{Ga} \gtrsim 80$ for fluvial transport ($s \lesssim 10$) and $s^{1/2}\text{Ga} \gtrsim 200$ for aeolian transport ($s \gtrsim 10$). The line corresponds to Eq. (1).

vast majority of nonsuspended sediment transport conditions that occur in nature, including sand and gravel transport in water and air on Venus, Titan, Earth, Mars, and Pluto.

Equation (1) contains a linear and a quadratic term in M_*. The linear term dominates when only a few particles are transported ($M_* \ll 1/c_M$), that is, when the bed can be considered quasistatic and not many binary collisions between transported particles occur. The quadratic term becomes important once $M_* \sim 1/c_M$, that is, once binary collisions between transported particles become significant. Below, we show that Eq. (1) follows naturally from a rigorous link between momentum transport and fluctuation energy dissipation, in which the linear term corresponds to dissipation by fluid drag and particle-bed collisions and the quadratic term to dissipation in binary collisions.

For a single particle of mass m and velocity $\mathbf{v}$ subjected to the force $\mathbf{F}$, Newton's axiom $\mathbf{F} = m\dot{\mathbf{v}}$ dictates $(d/dt)\frac{1}{2}mv_z v_x = F_{(x}v_{z)}$, where the parentheses denote the symmetrization of the indices. This balance relates the horizontal particle momentum to the contact (superscript c) and fluid drag (superscript d) forces acting on the particle via $\frac{1}{2}mv_x\tilde{g} = -F_{(x}^{\tilde{g}}v_{z)} = F_{(x}^c v_{z)} + F_{(x}^d v_{z)} - (d/dt)\frac{1}{2}mv_z v_x$. Summing over all particles per unit bed area and time averaging then yields (steady, homogenous transport conditions)

$$\frac{1}{2}Q_* = D_*^c + D_*^d, \tag{2}$$

where $(D_*^c, D_*^d) \equiv (D^c, D^d)/(\rho_p \tilde{g}d\sqrt{s\tilde{g}d})$, with $D^c \equiv (1/\Delta)\langle \sum_i F_{(x}^{ci}v_{z)}\rangle_T$ and $D^d \equiv (1/\Delta)\langle \sum_i F_{(x}^{di}v_{z)}\rangle_T$ the dissipation rates per unit bed area by particle contact and fluid drag forces, respectively, of $-(1/\Delta)\langle \sum_i \frac{1}{2}m^i v_z^i v_x^i \rangle_T$ [26], which physically represents a fluctuation energy because $\langle \sum_i m^i v_z^i \rangle_T = 0$ in the steady state [28].

For any elevation z, D^c can be separated into the contact dissipation rate $D^{c\uparrow}(z) \equiv (1/\Delta)\langle \sum_{z^i \geq z} F_{(x}^{ci}v_{z)}\rangle_T$ of particles moving above z and the contact dissipation rate $D^{c\downarrow}(z) \equiv (1/\Delta)\langle \sum_{z^i < z} F_{(x}^{ci}v_{z)}\rangle_T$ of particles moving below z, that is, $D^c = D^{c\uparrow}(z) + D^{c\downarrow}(z)$. We find that, for any given transport condition, there is an elevation z_c such that $D_*^{c\uparrow}(z_c) = a_c M_*^2$ and $D_*^{c\downarrow}(z_c) = b_c M_*$, where a_c and b_c are parameters independent of M_* (see Fig. 2 for two exemplary cases). In the region $z \geq z_c$, energy is predominantly dissipated in binary particle collisions, and thus the scaling with M_*^2 expresses the binary collision probability (analogous to granular kinetic theory [29]). In the region $z < z_c$, the sediment bed is quasistatic and energy dissipation is controlled by the probability of particle-bed collisions, which scales with M_*. Furthermore, for the relevant transport conditions (legend of Fig. 1), we find that the drag dissipation rate D_*^d roughly scales with the
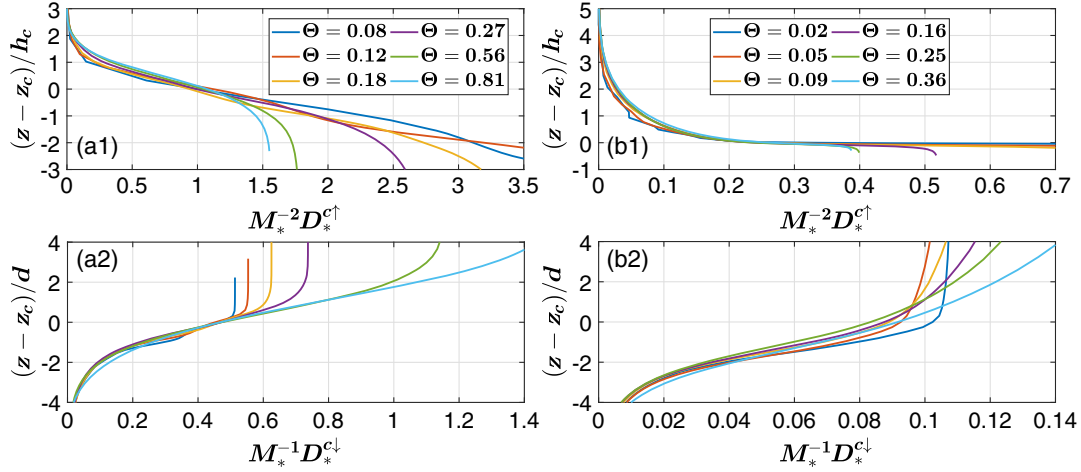
FIG. 2. Vertical profiles of $M_*^{-2}D_*^{c\uparrow}$ [(a1) and (b1)] and $M_*^{-1}D_*^{c\downarrow}$ [(a2) and (b2)]. Profiles in (a1) and (b1) are rescaled by the transport layer thickness above z_c: $h_c \equiv \int_{z_c}^{\infty} \phi z \, dz / \int_{z_c}^{\infty} \phi \, dz - z_c$, where ϕ is the particle volume fraction. Lines correspond to data from numerical sediment transport simulations for an exemplary fluvial transport condition [density ratio $s = 2.65$, Galileo number Ga = 50, and various Shields numbers Θ; (a1) and (a2), figure legend in (a1)] and an exemplary aeolian transport condition [$s = 2000$, Ga = 5, and various Θ; (b1) and (b2), figure legend in (b1)].

sediment mass that is responsible for the fluctuation motion (i.e., transported particles), that is, $D_*^d = a_d M_*$, where a_d is a parameter that is roughly independent of M_* [26]. Hence, the total dissipation rate ($D_*^c + D_*^d$) scales as

$$\frac{1}{2}Q_* = D_*^c + D_*^d = (a_c + a_d)M_* + b_c M_*^2. \quad (3)$$

Using the definition $\overline{v_{x*}} = Q_*/M_*$ and taking the limit $M_* \to 0$ (i.e., $\Theta \to \Theta_t$), we obtain the closure relation $2(a_c + a_d) = \overline{v_{x*}}(M_* \to 0) \equiv \overline{v_{x*t}}$. Furthermore, the strength of the nonlinear term [c_M in Eq. (1)] is given by the ratio of the fluctuation energy dissipated in binary collisions and that dissipated by fluid drag and particle-bed collisions: $c_M = b_c/(a_c + a_d)$. Note that, although b_c and $a_c + a_d$

are in general functions of Ga and s, their ratio c_M is approximately constant for relevant conditions (Fig. 1).

We further simplify Eq. (1) using two insights: (i) steady, homogeneous transport states are those at which M_* is so large that the flow (weakened by the particle-flow feed-back) is *barely* able to compensate the average energy losses of transported particles rebounding with the bed [22], and (ii) Θ_t is the smallest Shields number for which such a state exists [20,21]. These insights allow para-metrizing $\overline{v_{x*t}}$ and M_* in terms of the Shields number Θ as $\overline{v_{x*t}} = 2\kappa^{-1}\sqrt{\Theta_t}$ (valid for $s^{1/4}\mathrm{Ga} \gtrsim 40$) and $M_* = \mu_b^{-1}(\Theta - \Theta_t)$ [26], where $\kappa = 0.4$ is the von Kármán constant and μ_b an approximately constant bed friction coefficient that characterizes the geometry of particle-bed rebounds (we choose $\mu_b = 0.63$, which yields reasonable
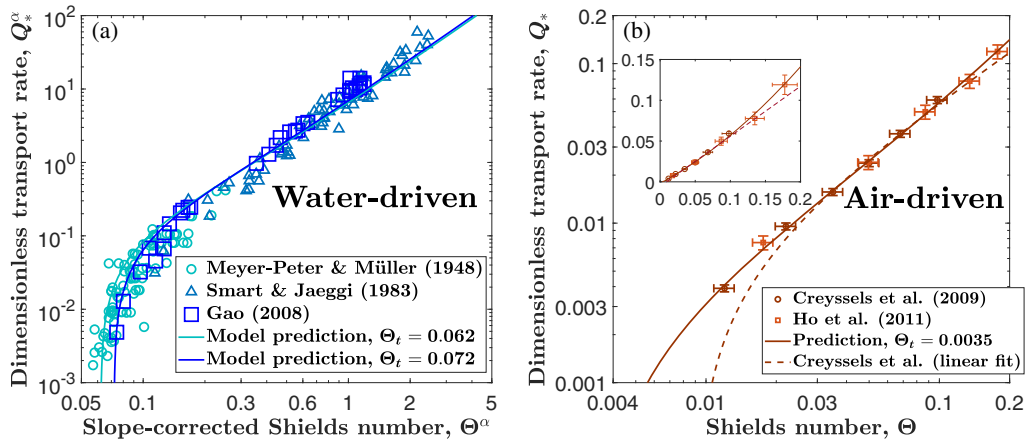
FIG. 3. Test of Eq. (4) (solid lines) against laboratory measurements of nonsuspended sediment transport driven by (a) water [16–18] and (b) air on Earth [13,14]. Raw measurements of Ref. [18] (as reported in Ref. [34]) and Ref. [17] are corrected for sidewall drag using the method of Ref. [35] and afterward slope-corrected through Eq. (5). Measurement data of Ref. [16] (mild bed slopes) are as reported in that reference and not further corrected.

overall agreement with the simulation data [26]). Equation (1) then becomes

$$Q_* = \frac{2\sqrt{\Theta_t}}{\kappa\mu_b}(\Theta - \Theta_t)\left[1 + \frac{c_M}{\mu_b}(\Theta - \Theta_t)\right], \quad (4)$$

where we neglect potential effects of particle shape and size distribution on c_M and μ_b.

Equation (4) exhibits two extreme regimes, a linear scaling $Q_* \sim (\Theta - \Theta_t)$ for $(\Theta - \Theta_t) \ll \mu_b/c_M$ (typical for aeolian transport) and a quadratic scaling $Q_* \sim \Theta^2$ for $(\Theta - \Theta_t) \gg \mu_b/c_M$ (typical for intense fluvial transport). The latter scaling is consistent with two-phase flow models of intense transport [30–33]. For intermediate values $(\Theta - \Theta_t) \sim \mu_b/c_M$, one can approximate $1 + c_M(\Theta - \Theta_t)/\mu_b \approx 2\sqrt{c_M(\Theta - \Theta_t)/\mu_b}$, implying $Q_* \sim (\Theta - \Theta_t)^{3/2}$, which is one the most widely used scaling laws in hydraulic engineering for the transport of gravel by water [16]. Note that Eq. (4) requires continuous transport conditions to be strictly valid (i.e., $\Theta \gtrsim 2\Theta_t$) [1]. In particular, it is expected to underestimate measurements for $\Theta \lesssim \Theta_t$ (for which it predicts $Q_* = 0$) and overestimate measurements for $\Theta_t \lesssim \Theta \lesssim 2\Theta_t$ [1].

In order to compare Eq. (4), which has been derived for a bed slope angle $\alpha = 0$, with slope-driven transport experiments in water (i.e., $\tau = \rho_f gh\sin\alpha$, where h is the clear-water depth), one has to replace Θ (but not Θ_t) and Q_*^2 in Eq. (4) by [26]

$$(\Theta^\alpha, Q_*^{\alpha 2}) \equiv (\Theta, Q_*^2)\Big/\left(\cos\alpha - \frac{\sin\alpha}{\mu_b}\frac{s}{s-1}\right). \quad (5)$$

When applying this correction and using transport threshold values that are close to (water) or equal to (air) those obtained from a recent threshold model [21], Eq. (4) simultaneously reproduces laboratory measurements of the rate of continuous transport in water [Fig. 3(a)] and air on Earth [Fig. 3(b)]. In particular, the agreement with aeolian transport measurements is substantially better than the old fitted linear model [13]. Equation (4) is also consistent with numerical simulations (Fig. 4).

The applicability of Eq. (4) is limited to transport conditions that exceed critical values of $s^{1/2}$Ga and $s^{1/4}$Ga. The number $s^{1/4}$Ga determines whether transported particles tend to move predominantly within the log-layer [$s^{1/4}$Ga $\gtrsim 40$, as required for Eq. (4)] or within the viscous sublayer of the turbulent boundary layer ($s^{1/4}$Ga $\lesssim 40$), while $s^{1/2}$Ga characterizes the importance of particle inertia relative to viscous drag forcing [21,36]. When $s^{1/2}$Ga is too small [$s^{1/2}$Ga $\lesssim 80$ for fluvial transport ($s \lesssim 10$) and $s^{1/2}$Ga $\lesssim 200$ for aeolian transport ($s \gtrsim 10$)], the scaling of the fluid drag dissipation rate of kinetic particle fluctuation energy changes due to strong viscous drag forcing, causing substantial deviations from Eq. (4). Likewise, we expect Eq. (4) to break down when the
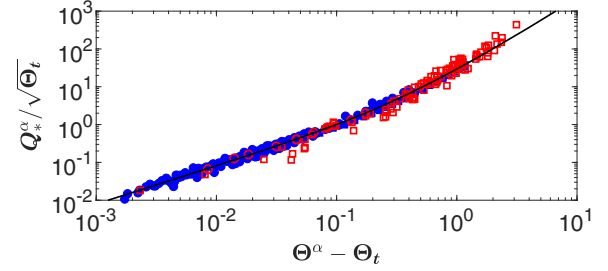
FIG. 4. Test of Eq. (4) (solid line) against numerical simulations (blue symbols, cf. Fig. 1) and laboratory measurements (red symbols, cf. Fig. 3) of nonsuspended aeolian (circles) and fluvial (squares) sediment transport. Only those simulation data of Fig. 1 are shown that obey $s^{1/2}$Ga $\gtrsim 40$ [validity requirement for Eq. (4)]. The shown fluvial data do not include measurements of Ref. [16] for visibility reasons.

bed slope angle α comes close to the angle of repose α_r, that is, when previous studies suggest that sediment transport properties change relatively abruptly [37].

In this Letter, we have shown that the manner in which kinetic particle fluctuation energy is dissipated controls the scaling of the rate Q of continuous nonsuspended sediment transport with the fluid shear stress τ applied onto the bed. In particular, this scaling becomes nonlinear once fluctuation energy dissipation in binary particle collisions, as opposed to dissipation in particle-bed collisions and via fluid drag, becomes significant. This new physical picture replaces an old, widely accepted hypothesis about the physical origin of the scaling differences of Q. Previously, it was hypothesized that a different predominant mode of bed sediment entrainment is responsible for these differences [2–5,20,38]: entrainment caused by the impacts of transported particles onto the bed ("splash" [39–41]) in aeolian transport versus entrainment caused by the direct action of fluid forces in fluvial transport. However, a number of recent independent studies revealed that impact entrainment plays a crucial role also in fluvial transport [1,36,42–46], making it clear that a better supported hypothesis was needed.

Our physical description has culminated in an expression for Q that unifies transport in water and air streams without fitting to experimental data. In combination with a previous unification of the aeolian and fluvial transport threshold [21], we are now able to estimate planetary sediment transport and the evolution of planetary sediment surfaces much more reliably than before.

---

*0012136@zju.edu.cn
[1] T. Pähtz, A. H. Clark, M. Valyrakis, and O. Durán, The physics of sediment transport initiation, cessation, and

entrainment across aeolian and fluvial environments, Rev. Geophys. **58,** e2019RG000679 (2020).

[2] M. H. Garcia, *Sedimentation Engineering: Processes, Measurements, Modeling, and Practice* (American Society of Civil Engineers, Reston, VA, 2008).

[3] C. Ancey, Bedload transport: A walk between randomness and determinism. Part 1. The state of the art, J. Hydraul. Eng. **58,** 1 (2020).

[4] O. Durán, P. Claudin, and B. Andreotti, On aeolian transport: Grain-scale interactions, dynamical mechanisms and scaling laws, Aeolian Res. **3,** 243 (2011).

[5] J. F. Kok, E. J. R. Parteli, T. I. Michaels, and D. B. Karam, The physics of wind-blown sand and dust, Rep. Prog. Phys. **75,** 106901 (2012).

[6] R. A. Bagnold, *The Physics of Blown Sand and Desert Dunes* (Methuen, New York, 1941).

[7] M. C. Bourke, N. Lancaster, L. K. Fenton, E. J. R. Parteli, J. R. Zimbelman, and J. Radebaugh, Extraterrestrial dunes: An introduction to the special issue on planetary dune systems, Geomorphology **121,** 1 (2010).

[8] F. Charru, B. Andreotti, and P. Claudin, Sand ripples and dunes, Annu. Rev. Fluid Mech. **45,** 469 (2013).

[9] P. Claudin and B. Andreotti, A scaling law for aeolian dunes on Mars, Venus, Earth, and for subaqueous ripples, Earth Planet. Sci. Lett. **252,** 30 (2006).

[10] T. Pähtz, J. F. Kok, E. J. R. Parteli, and H. J. Herrmann, Flux Saturation Length of Sediment Transport, Phys. Rev. Lett. **111,** 218002 (2013).

[11] T. Pähtz, E. J. R. Parteli, J. F. Kok, and H. J. Herrmann, Analytical model for flux saturation in sediment transport, Phys. Rev. E **89,** 052213 (2014).

[12] T. Pähtz, A. Omeradžić, M. V. Carneiro, N. A. M. Araújo, and H. J. Herrmann, Discrete element method simulations of the saturation of aeolian sand transport, Geophys. Res. Lett. **42,** 2063 (2015).

[13] M. Creyssels, P. Dupont, A. Ould El Moctar, A. Valance, I. Cantat, J. T. Jenkins, J. M. Pasini, and K. R. Rasmussen, Saltating particles in a turbulent boundary layer: Experiment and theory, J. Fluid Mech. **625,** 47 (2009).

[14] T. D. Ho, A. Valance, P. Dupont, and A. O. El Moctar, Scaling Laws in Aeolian Sand Transport, Phys. Rev. Lett. **106,** 094501 (2011).

[15] R. L. Martin and J. F. Kok, Wind-invariant saltation heights imply linear scaling of aeolian saltation flux with shear stress, Sci. Adv. **3,** e1602569 (2017).

[16] E. Meyer-Peter and R. Müller, Formulas for bedload transport, in *Proceedings of the 2nd Meeting of the International Association for Hydraulic Structures Research* (IAHR, Stockholm, 1948), pp. 39–64.

[17] G. M. Smart and M. N. R. Jaeggi, Sediment transport on steep slopes, in *Mitteilungen der Versuchsanstalt für Wasserbau, Hydrologie und Glaziologie* (ETH Zurich, Zurich, Switzerland, 1983), p. 64.

[18] P. Gao, Transition between two bed-load transport regimes: Saltation and sheet flow, J. Hydraul. Eng. **134,** 340 (2008).

[19] H. Capart and L. Fraccarollo, Transport layer structure in intense bed-load, Geophys. Res. Lett. **38,** L20402 (2011).

[20] D. Berzi, J. T. Jenkins, and A. Valance, Periodic saltation over hydrodynamically rough beds: aeolian to aquatic, J. Fluid Mech. **786,** 190 (2016).

[21] T. Pähtz and O. Durán, The cessation threshold of non-suspended sediment transport across aeolian and fluvial environments, J. Geophys. Res. **123,** 1638 (2018).

[22] T. Pähtz and O. Durán, Universal friction law at granular solid-gas transition explains scaling of sediment transport load with excess fluid shear stress, Phys. Rev. Fluids **3,** 104302 (2018).

[23] O. Durán, B. Andreotti, and P. Claudin, Numerical simulation of turbulent sediment transport, from bed load to saltation, Phys. Fluids **24,** 103306 (2012).

[24] O. Durán, B. Andreotti, and P. Claudin, Turbulent and viscous sediment transport - a numerical study, Adv. Geosci. **37,** 73 (2014).

[25] O. Durán, P. Claudin, and B. Andreotti, Direct numerical simulations of aeolian sand ripples, Proc. Natl. Acad. Sci. U.S.A. **111,** 15665 (2014).

[26] See the Supplemental Material at http://link.aps.org/supplemental/10.1103/PhysRevLett.124.168001 for numerical model details, the computation of particle properties from the simulation data, derivation details, drag dissipation, parametrizations of M_* and $\overline{v_{x*t}}$, and slope correction.

[27] M. Yalin, *Mechanics of Sediment Transport* (Pergamon Press, Oxford, 1977).

[28] T. Pähtz, O. Durán, T.-D. Ho, A. Valance, and J. F. Kok, The fluctuation energy balance in non-suspended fluid-mediated particle transport, Phys. Fluids **27,** 013303 (2015).

[29] V. Kumaran, Kinetic theory for sheared granular flows, C. R. Phys. **16,** 51 (2015).

[30] J. M. Pasini and J. T. Jenkins, Aeolian transport with collisional suspension, Proc. R. Soc. A **363,** 1625 (2005).

[31] D. Berzi and L. Fraccarollo, Inclined, collisional sediment transport, Phys. Fluids **25,** 106601 (2013).

[32] J. Chauchat, A comprehensive two-phase flow model for unidirectional sheet-flows, J. Hydraul. Res. **56,** 15 (2018).

[33] R. Maurin, J. Chauchat, and P. Frey, Revisiting slope influence in turbulent bedload transport: Consequences for vertical flow structure and transport rate scaling, J. Fluid Mech. **839,** 135 (2018).

[34] P. Gao, Mechanics of bed load transport in the saltation and sheetflow regimes, Ph.D. thesis, State University of New York, Buffalo, New York, USA, 2003.

[35] G. P. Williams, Flume width and water depth effects in sediment-transport experiments, in *US Geological Survey Professional Paper 562-H* (U.S. Government Printing Office, Washington, D.C., 1970).

[36] T. Pähtz and O. Durán, Fluid forces or impacts: What governs the entrainment of soil particles in sediment transport mediated by a Newtonian fluid? Phys. Rev. Fluids **2,** 074303 (2017).

[37] T. Loiseleux, P. Gondret, M. Rabaud, and D. Doppler, Onset of erosion and avalanche for an inclined granular bed sheared by a continuous laminar flow, Phys. Fluids **17,** 103304 (2005).

[38] B. Andreotti, A two-species model of aeolian sand transport, J. Fluid Mech. **510,** 47 (2004).

[39] D. Beladjine, M. Ammi, L. Oger, and A. Valance, Collision process between an incident bead and a three-dimensional granular packing, Phys. Rev. E **75,** 061305 (2007).

[40] F. Comola and M. Lehning, Energy- and momentum-conserving model of splash entrainment in sand and snow saltation, Geophys. Res. Lett. **44**, 1601 (2017).

[41] M. Lämmel, K. Dzikowski, K. Kroy, L. Oger, and A. Valance, Grain-scale modeling and splash parametrization for aeolian sand transport, Phys. Rev. E **95**, 022902 (2017).

[42] B. Vowinckel, R. Jain, T. Kempe, and J. Fröhlich, Entrainment of single particles in a turbulent open-channel flow: A numerical study, J. Hydraul. Res. **54**, 158 (2016).

[43] A. H. Clark, M. D. Shattuck, N. T. Ouellette, and C. S. O'Hern, Onset and cessation of motion in hydrodynamically sheared granular beds, Phys. Rev. E **92**, 042202 (2015).

[44] A. H. Clark, M. D. Shattuck, N. T. Ouellette, and C. S. O'Hern, Role of grain dynamics in determining the onset of sediment transport, Phys. Rev. Fluids **2**, 034305 (2017).

[45] J. Heyman, P. Bohorquez, and C. Ancey, Entrainment, motion, and deposition of coarse particles transported by water over a sloping mobile bed, J. Geophys. Res. **121**, 1931 (2016).

[46] D. B. Lee and D. Jerolmack, Determining the scales of collective entrainment in collision-driven bed load, Earth Surf. Dyn. **6**, 1089 (2018).